Comparison of some wind turbine noise emission models coupled to BEM aerodynamics

IOP Conf. Series: Journal of Physics: Conf. Series **1037** (2018) 022038 doi:10.1088/1742-6596/1037/2/022038

Comparison of some wind turbine noise emission models coupled to BEM aerodynamics

CR Sucameli[1], P Bortolotti[1], A Croce[2] and CL Bottasso[1,2]

[1] Wind Energy Institute, Technische Universität München, Garching, Germany
[2] Department of Aerospace Science and Technology, Politecnico di Milano, Milano, Italy

E-mail: carlo.bottasso@tum.de

Abstract. Noise is an important design driver for onshore wind turbines. Therefore, there is a need to include validated noise prediction models within wind turbine and wind plant design procedures. However, the literature presents a multitude of different models and formulations, combined with a severe lack of publicly available experimental data. The present work presents a comparison between semi-empirical frequency-domain methods coupled to blade element momentum (BEM) aerodynamics, which is the typical approach used for the transient aeroelastic analysis of wind turbines. Among the various noise sources, only turbulent boundary layer – trailing edge and turbulent inflow noise models have been considered in the present analysis. The noise models are benchmarked in terms of emission spectra, highlighting differences and discrepancies. A time-domain Ffowcs Williams-Hawkings formulation is also coupled to the same BEM model, investigating its ability in predicting low frequency emissions. Thanks to this study, a few inconsistencies among published noise models are identified and reported.

1. Introduction

Noise emitted by wind turbines is an important constraint to the penetration of onshore wind in the energy mix. As a consequence, noise is gaining an increasing importance within the area of wind turbine design [1]. To this end, there is a need for reliable and validated noise emission models that can be adopted within integrated design procedures. Although high-fidelity first-principle models are indispensable, the integration of noise within a design environment calls for methods of moderate computational complexity.

While quite a few authors have dealt with the topic of wind turbine noise modeling, the literature is characterized by different models and various formulations of each model, combined with a severe lack of experiments where both noise and wind turbine data are fully publicly available. These two aspects call for a consistent review of available models together with their validation with respect to experimental data. The present paper is concerned with the first of these two problems, offering a review and comparison of various formulations. This is achieved by implementing different well known aeroacoustic models coupled to the aeroservoelastic wind turbine solver `Cp-Lambda` [2]. `Cp-Lambda` implements a blade element momentum (BEM) formulation, and it provides the aeroelastic simulation needs of the wind turbine design framework `Cp-Max` [3].

Wind turbine noise models can be categorized into two families: frequency- and time-domain methods. The models of the first group are usually coupled to BEM aerodynamics and are summarized in Sect. 2. Here, a brief description of the noise sources included in the present

analysis is also presented. Time-domain methods are based on acoustic analogies and within this category the Ffowcs Williams-Hawkings [4] (FW-H) model is included in this work. In wind energy applications, the FW-H formulation has so far been mostly used to calculate sound propagation from near-field data computed through 3D CFD simulations. Since the use of CFD within design optimization is hampered by its excessive computational cost, the present study investigates the coupling of the FW-H formulation with the BEM-based `Cp-Lambda` model. This coupling is presented in Sect. 3. The work is closed with a discussion on the results, which are reported in Sect. 4, and by conclusions and an outlook on the next steps, which are given in Sect. 5.

2. Frequency-domain methods

Frequency-domain methods are semi-empirical models that describe different noise mechanisms, typically grouped into self-noise and turbulent inflow (TI) noise. Self-noise is generated from the interaction of an airfoil with its boundary layer and near wake, being then "self-produced". This group of noise sources was first modeled in 1989 by Brooks, Pope and Marcolini [5], who distinguished between turbulent boundary layer – trailing edge (TBL-TE), laminar boundary layer – vortex shedding, trailing edge bluntness, separation-stall and tip noise. An extensive experimental campaign was conducted on NACA0012 airfoils of different chords, operating at different flow speeds and angles of attack. This activity lead to the definition of a semi-empirical model, commonly named BPM. Thanks to its simplicity, the BPM model is still widely used within the wind energy industry. Given however the empirical nature of the model, its main drawback is its limited applicability to other airfoils and flow conditions.

Among the various noise sources, TBL-TE noise and TI noise are typically identified as particularly relevant in modern pitch-regulated wind turbines [6]. These are therefore the ones specifically considered in this work. Sections 2.1 and 2.2 discuss the various formulations presented in the literature for these two noise generation mechanisms.

2.1. Turbulent boundary layer – trailing edge noise

TBL-TE noise arises from the interaction of eddies of various size with the trailing edge of an airfoil, causing the generation of pressure fluctuations that propagate to the far field. Considerable effort has been dedicated in the past decades to the development and validation of TBL-TE noise prediction models, leading today to a good availability of experimental and numerical results [7, 8].

As already stated above, the first method for estimating TBL-TE noise is the BPM model that, thanks to its simplicity and to recent upgrades [9], is still routinely used in noise assessments. Recently, a more physical model for TBL-TE noise has been developed by Parchen [10] at the Dutch research institute TNO. This model, which is here labeled "TNO", combines theories for the computation of surface pressure fluctuations and far-field sound spectrum prediction from Chandiramani [11], Chase [12] and Blake [13]. This model has been studied and further improved by multiple authors [14, 15, 16], and it has also been extended by different studies to take into account the anisotropy of the boundary layer in proximity of the trailing edge [17, 18].

Both BPM and TNO models require the computation of boundary layer parameters on the suction and pressure sides of the airfoil. This information can be estimated either from CFD simulations or by boundary layer solvers. In the present work, the viscous-inviscid 2D panel code `XFOIL` [19] is used, which includes the possibility of setting a forced or free transition (computed through an e^N transition criterion). Blade tripping may have a potential impact on trailing edge noise [6, 20]. However, in the present study no trip of the blade was imposed, and the free transition exponent was set to $N = 9$.

Table 1: Comparison dataset for BPM validation

Parameter	**Data**
Airfoil	NACA0012
Section span	0.45 m
Chord	0.30 m
Freestream velocity	71.3 m/s
Distance source-observer	1.22 m

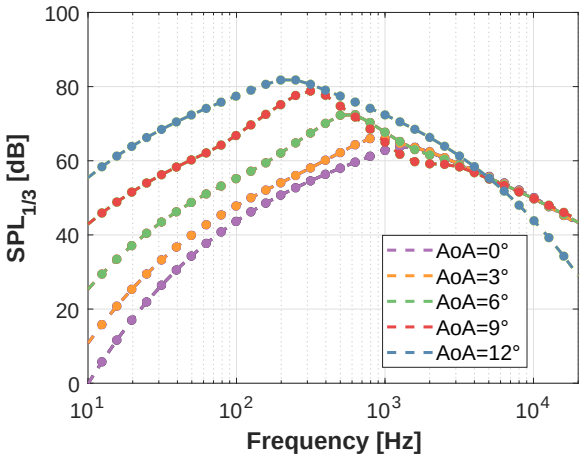

Figure 1: BPM Comparison

Outputs of the BPM model are calculated in terms of 1/3 octave band discretization sound pressure level $SPL_{1/3}$, obtained by the sum of three different terms

$$SPL_{TOT} = 10\log(10^{SPL_\alpha/10} + 10^{SPL_p/10} + 10^{SPL_s/10}), \tag{1}$$

where the terms SPL_p, SPL_s, SPL_α are, respectively, the contributions to the sound pressure level given by the airfoil pressure side, suction side and by the angle of attack. These terms respectively write

$$SPL_p = 10\log\left(\frac{\delta_p^* M^5 L D_h}{R^2}\right) + A\left(\frac{St_p}{St_1}\right) + (K_1 - 3) + \Delta K_1, \tag{2a}$$

$$SPL_s = 10\log\left(\frac{\delta_s^* M^5 L D_h}{R^2}\right) + A\left(\frac{St_s}{St_1}\right) + (K_1 - 3), \tag{2b}$$

$$SPL_\alpha = 10\log\left(\frac{\delta_s^* M^5 L D_h}{R^2}\right) + B\left(\frac{St_s}{St_1}\right) + K_2, \tag{2c}$$

with A and B functions of the Strouhal number, δ^* the boundary layer displacement thickness, M the incident Mach number, L the section span and R the distance between source and observer. The directivity function D_h is discussed later and reported in Eq. 8. For brevity, the details of the implementation are not given here, but interested readers can refer to [5].

The implementation of the BPM model is benchmarked against NREL's aeroacoustic software `NAFNoise` [21], which also includes the BPM model. The analysis is performed for the dataset reported in Table 1 at various angles of attack, where the observer is placed vertically above the trailing edge. Figure 1 shows the perfect agreement obtained between `NAFNoise` (dotted lines) and `Cp-Max` (markers).

The computation of noise spectra in the TNO model follows a different approach. First, surface pressure fluctuation spectra at the trailing edge are computed by the following equation

$$P(k_1, k_3, \omega) = 4\rho_0^2 \frac{k_1^2}{k_1^2 + k_3^2} \int_0^\delta 2L_2(x_2)\overline{u_2^2}\left(\frac{\partial U_1}{\partial x_2}\right)^2 \Phi_{22}(k_1, k_3, \omega) \times \Phi_m(\omega - U_c(x_2)k_1) e^{(-2|\vec{k}|y_2)} \mathrm{d}x_2, \tag{3}$$

where indices $1, 2, 3$ correspond to the streamwise, normal to the airfoil plane and spanwise directions, respectively. In Eq. 3, δ is the boundary layer thickness, L_2 is the vertical integral

length scale, $\overline{u_2^2}$ is the vertical velocity Reynolds stress component, U_1 is the mean velocity in the turbulent boundary layer, which has been approximated using Cole's law of the wall as reported in [15]. In addition, Φ_{22} is the vertical velocity fluctuation spectrum, Φ_m is the moving axis spectrum —modeled here as a Dirac delta—, U_c is the convection velocity of eddies along the trailing edge and finally $\vec{k} = (k_1, k_2, k_3)$ identifies the wave-number vector. The computation of the surface pressure spectrum follows the approach explained in [22], which includes different vertical integral turbulent lengths and turbulence spectra taking into account the anisotropy of the boundary layer derived in a previous work [17].

The far-field spectrum is computed from the surface pressure fluctuation spectrum according to [23], i.e.

$$S_{pp}(\omega) = \frac{2L}{\pi R^2} D \int_{-\infty}^{+\infty} \frac{\omega}{c_0 |\vec{k} \cdot \vec{n}|} \frac{P(k_1, k_3, \omega)}{(1 - M_{v,R})^2 (1 - M_{v,1} \sin\phi)} \mathrm{d}k_1, \tag{4}$$

where $M_{v,R}$ is the component of the eddy velocity Mach number in the observer direction and $M_{v,1}$ the projection of the eddy convection Mach number along the chord. In the present work, the eddy velocity Mach number M_v is computed as the wind speed at the outer edge of the boundary layer. The relative position between source and observer is identified through the angles ϕ and θ, shown in Fig. 2. Finally, the term D represents the directivity factor, defined as

$$D = \frac{\sin\phi \sin^2(\theta/2)}{(1 + M \sin\phi \cos\theta)^2 (1 - M_W \sin\phi \cos\theta)^2}, \tag{5}$$

where M is the incident Mach number on the airfoil and M_W is the wake convection one, here computed as

$$M_W = M \frac{\int_0^\delta U_1(x_2) \mathrm{d}x_2}{U_\infty \delta}, \tag{6}$$

with $U_1(x_2)$ defined as the chordwise component of the velocity in the boundary layer (as in Eq. 4).

Alternatively, far-field computations can follow the approach taken by Bertagnolio et al. [22], which adopts a different directivity factor. Here, the sound spectrum is calculated according to Brooks and Hodgson [24], which is valid for low Mach numbers and writes

$$S_{pp}(\omega) = \frac{D_h L}{4\pi R^2} \int_{-\infty}^{+\infty} \frac{\omega}{c_0 k_1} P(k_1, k_3 = 0, \omega) \mathrm{d}k_1, \tag{7}$$

where D_h is now a different directivity factor, similar to the one employed in the BPM model for high frequency noise

$$D_h = \frac{2 \sin^2\phi \sin^2(\theta/2)}{(1 + M \cos\theta)^3}. \tag{8}$$

It must be noted that the two directivities shown in Eq. 5 and 8 are not based on the same coordinate system, and the reference system for the latter can be found in the original BPM publication [5]. For the remaining of the present paper, TNO-Howe refers to the former model, while TNO-DTU to the latter.

The ability of the implemented tools to predict noise emissions is verified by comparing with results reported by different researchers during the Third Workshop on Benchmark Problems for Airframe Noise Computations BANC-III [8]. Numerical methods used by benchmark participants range from very computationally intensive hybrid RANS/LES + FW-H far field propagation (PoliTo) to TNO models coupled to RANS simulation (IAG and DTU). A comprehensive description of numerical procedures and experimental settings can be found in the original publication [8]. Sound pressure levels in 1/3 octave band discretization are compared

and results are shown in Fig. 3 for a NACA0012 at $U_\infty = 56$ m/s, $Re = 1.50 \times 10^6$, $\alpha = 0$, $M_\infty = 0.1664$ (case 1 of the original publication). Spectra computed by the implemented TNO models seem to agree reasonably well with published results, correctly predicting the peak frequency and the overall trend of the spectra. Differences are however present. These are attributed to the assumptions made in the computation of the surface pressure fluctuation spectra from the `XFOIL` boundary layer input [15].

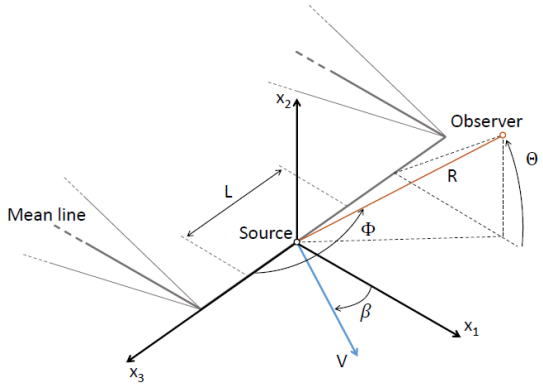

Figure 2: Directivity angles

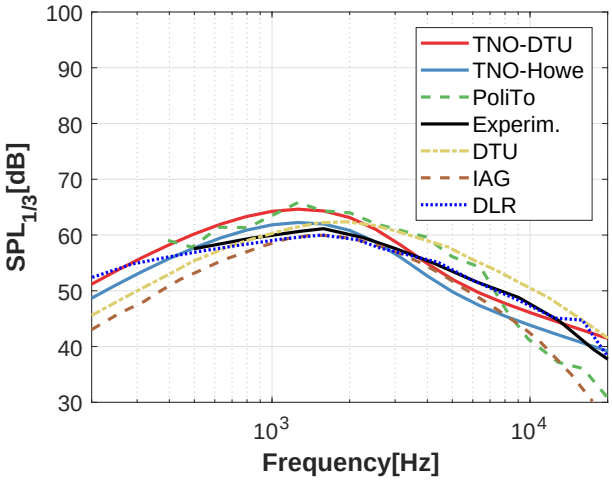

Figure 3: BANC III SPL comparison

2.2. Turbulent inflow noise

The second dominating source of noise generated by wind turbines is TI noise, which is produced by pressure oscillations following the unsteady loading generated on the blades due to the incoming wind turbulence. This noise source was first characterized by Amiet [25] and Paterson and Amiet [26], modeling the far field noise spectrum produced by a flat plate exposed to a turbulent flow. Modified versions of the Amiet model have been later developed by Lowson [27] and Moriarty et al. [16], among others. Corrections to take into account airfoil thickness have been obtained by Guidati et al., [28] and Roger et al. [29]. Approximate formulas to compute TI noise were also given by Amiet in his original work [25]. In the present work four different implementations of TI noise are compared, chosen as the most popular options among the many available ones.

In the first model, here labeled "TI Amiet-Paterson", TI is predicted using the Amiet and Paterson theory [26], which involves complex unsteady aerodynamics and computes the far-field sound spectrum as

$$S_{pp}(\vec{r},\omega) = \left(\frac{\omega x_3 \rho_0 b}{c_0 \sigma^2}\right) \pi U_\infty d |\mathcal{L}(\vec{r}, K_1, K_3)|^2 \tilde{\Phi}_{22}(K_1, K_3), \tag{9}$$

with b and d the semi-chord and semi-span of the airfoil, respectively, whereas $\mathcal{L}$ is the unsteady lift response and $\tilde{\Phi}_{22}$ the spectrum of turbulent velocity fluctuations in the direction normal to

the airfoil. The remaining terms are defined as

$$\sigma^2 = x_1^2 + \beta^2(x_2^2 + x_3^2), \tag{10a}$$
$$\beta^2 = 1 - M^2, \tag{10b}$$
$$K_1 = \frac{\omega}{U_\infty}, \tag{10c}$$
$$K_3 = \frac{\omega x_3}{c_0 \sigma}. \tag{10d}$$

A detailed explanation of the physics and implementation of the model can be found in the original publication. Appendix E of [26] reports approximate expressions for the computation of the far-field $SPL_{1/3}$ noise, discriminating between low and high frequency:

$$SPL_{\mathrm{Low},1/3} = 10\log\left(S^2\left(\frac{\overline{K}_x}{\beta^2}\right)\frac{M^6}{\beta^2}\overline{K}_1^2\frac{L_t d}{x_3^2}I^2\rho_0^2 c_0^4\frac{\hat{K}_1^3}{(1+\hat{K}_1^2)^{7/3}}\right) + 68.4, \tag{11a}$$

$$SPL_{\mathrm{High},1/3} = 10\log_{10}\left(\frac{L_t d}{x_3^2}M^5 I^2\frac{\hat{K}_1^3}{(1+\hat{K}_1^2)^{7/3}}\rho_0^2 c_0^4\right) + 58.4, \tag{11b}$$

where $\overline{K}_1 = K_1 b$, $\hat{K}_1 = K_1/k_e$, $k_e = 0.75 L_t$ is the wavenumber of energy containing eddies, while S approximates the Sears function

$$S^2 \approx \left(\frac{2\pi\overline{K}_x}{\beta^2} + \left(1 + 2.4\frac{\overline{K}_x}{\beta^2}\right)^{-1}\right)^{-1}. \tag{12}$$

The remaining terms of Eq. 11a are the turbulent length L_t and the turbulence intensity I, defined in the local frame. This model, which is just an approximation of the full Amiet-Paterson model reported above, is here labeled "TI Amiet". It must be noted that, according to the original implementation, ρ_0 and c_0 are not defined in SI units, but respectively in g/cm^3 and cm/s, and a redefinition of such quantities would require a change in the constants of both equations.

The third model implemented in this work, here termed "TI Lowson", is very similar to the TI Amiet model reported in Eq. 11b, but it includes a different definition of K_1 [27]:

$$SPL_{\mathrm{Tot},1/3} = SPL_{High,1/3} + 10\log_{10}\left(\frac{LFC}{1+LFC}\right), \tag{13a}$$

$$SPL_{\mathrm{High},1/3} = 10\log_{10}\left(\frac{L_t d}{R^2}M^3 u_{\mathrm{rms}}^2\frac{K_1^3}{(1+K_1^2)^{7/3}}\rho_0^2 c_0^2\right) + 58.4, \tag{13b}$$

$$LFC = 10 S^2 M\frac{\overline{K}_1^2}{\beta^2}, \tag{13c}$$

$$K_1 = \pi f c/U_\infty, \tag{13d}$$

where u_{rms} is the root mean square of the velocity fluctuations in the mean wind direction and LFC defines the low-frequency correction. The Lowson model has been implemented in several studies, although the original paper is not easily accessible in the public domain. Differences between the Lowson and Amiet models reside on the adimensionalization of the wavenumber (with respect to the mid-chord rather than the dimension of energy-containing eddies), a different definition of the turbulence intensity and of the units of measure used. Nevertheless, the original document does not highlight those differences nor does it report a derivation of the model from

the Amiet one. This may have led to the appearance in the literature of incomplete or incorrect formulations. For example, Zhu et al. [20] and Kim et al. [30] replace u_{rms} with I, while Botha et al. [31] presents an erroneous declaration of the terms and units of measure.

The last model considered here is very similar to the TI Amiet one, and it was developed by Moriarty [16] (here referred to as "TI Moriarty"). This model adopts the same high frequency approximation reported in Eq. 11b, coupled to the low frequency approximation given by Lowson in Eq. 13a, and it is implemented in the software `NAFNoise`.

All the turbulent inflow models rely on the definition of a turbulence intensity and integral length scale. As prescribed in IEC 61400-1 [32], the integral length scale is set here to vary linearly with height ($L_t = 0.7z$) up to 60 meters, above which it remains constant.

The aeroelastic code `Cp-Lambda` takes as input turbulent wind grids computed through the NREL's software `TurbSim` [33]. The computation of the turbulence intensity for the various models follows different approaches: the TI Amiet, TI Amiet-Paterson and TI Moriarty models calculate turbulence intensity locally on each span segment, extracting it from the time history of the relative wind speed of each airstation. In the TI Lowson formulation, turbulence intensity is instead computed directly from the wind grid input files. It should be here noted that wind speed time histories used for turbulence intensity computation are generated by `Cp-Lambda` and/or `TurbSim` at a fixed sampling frequency (typically set equal to 50 Hz). This means that these signals do not have the same frequency content of the whole acoustic frequency range (up to 20 kHz). The computation of the turbulence intensity is then necessarily only an approximation of the real one.

3. Time-domain method

Time-domain methods are based on acoustic analogies, which use manipulations of classical fluid dynamic equations to calculate acoustic pressures. In this work, the FW-H [4] model based on the Farassat 1A formulation [34] is implemented. This formulation requires the computation of thickness and loading noise on a control surface, neglecting the contribution of the quadrupole term of the original FW-H formulation. This way, the method can use as input the pressure and velocity distributions measured directly on the blade surface. These can be obtained from the combination of a BEM-based aeroelastic model such as `Cp-Lambda` and a boundary-layer software such as `XFOIL`. The latter is used to reconstruct pressure distributions on the blades from lift and drag coefficients. In this study, unsteady inflow effects are taken into account through a Pitt-Peters model [35]. Models of unsteady aerodynamics, such as the Onera stall model, are available, but have not been used in the present work.

It is clear that the frequency content of the computed acoustic pressure is directly linked to the space-time discretization of the aeroelastic solver. Using a standard discretization for wind grids, blade and time steps of the aeroelastic simulations, the FW-H method coupled to a BEM model can in principle model the low frequency noise associated to relatively large eddies of the flow. From a physical point of view, this corresponds to the low frequency spectrum of the turbulent inflow noise. The developed time-domain model presents the advantage of a very low computational effort, allowing the user to perform dozens of analysis in a matter of hours. Thanks to this, it would be feasible to use this model for infrasound assessments and design optimization studies.

It should be here however noted that several potentially important effects have so far been neglected. First, propagation phenomena such as sound absorption through air, ground reflection and modeling of wake effects are here not taken into account. Furthermore, as of now the tool is able to predict only the low-frequency noise associated to the rotor surface, while the effect of the tower on the flow is included in the current framework through a potential model. Sound generated from an unsteady pressure distribution induced by the rotor along the tower is therefore neglected.

4. Workflow and comparisons

Within the current simulation framework, the computation of frequency-based noise spectra is performed following several steps. First, boundary layer data at the trailing edge is computed by using `XFOIL`. For the various airfoils adopted along the blade span, data is stored in the form of three-dimensional lookup tables (including angle of attack, Reynolds and Mach). Aeroelastic simulations are then performed running `Cp-Lambda` and the rotor blades are discretized in several segments along the span. A sensitivity study shows that 12 segments equally spaced from 50% (mid-span) to 98% (tip) are needed to achieve convergence. Next, the retarded configuration for a set of observation times is calculated and boundary layer characteristics are retrieved through a lookup table interrogation, enabling the computation of noise spectra with the various models discussed in Sect. 2. Finally, noise spectra from the different instants of time are azimuthally averaged following the approach of Amiet-Schlinker [36]. This allows one to take into account the Doppler shifting of the noise sources.

For the FW-H model, the computation of acoustic pressure time histories follows a slightly different approach. Here, blade configurations and their associated aerodynamic loading are retrieved from the aeroelastic simulations. Then, blades are meshed using rectangular elements (50 in the spanwise and 30 in the chordwise directions) and pressure distributions along the blades are calculated with `XFOIL`. Lastly, the computation of the retarded configuration is performed for each observation time: inputs required by the Farassat 1A formulation are evaluated on the four-nodes Gauss points of each element, while integrals are evaluated numerically using Gaussian quadrature.

A comparison of all models is conducted by simulating the noise emissions of the reference 3.35 MW onshore wind turbine developed within IEA Wind Task 37 [37]. Noise spectra are computed at 7 and 11 m/s with a turbulence intensity of the wind grid equal to 10%. A time window of 60 seconds is used for the measurements. A summary of the configurational data of the wind turbine and details of the test cases are reported in Tables 2 and 3, respectively. Comparisons in terms of non-weighted SPL results obtained with frequency-based models are shown in Fig. 4. Here the observer is positioned as prescribed by IEC 61400-11 [38], namely downwind on the ground at a distance of hub height plus rotor radius. Visibly, the BPM model results differ considerably from the TNO ones. To investigate this phenomenon, a comparison on the aeroacoustic emissions of single airfoil sections is performed. This returns a good agreement between the two models when compared to the original BPM dataset. The match however rapidly deteriorates outside of the BPM experimental fitting boundaries (e.g. at higher Reynolds number or high incidence angles).

Regarding the turbulent inflow noise, the results from the TI Moriarty and TI Amiet models match well except in the lower portion of the spectrum, where minor differences are observed. These are due to the different low frequency approximations adopted by the two methods. Lastly, a dominating trend of turbulent inflow noise at low frequencies is observed. It can be noted from Fig. 4 that all the turbulent inflow model spectra present the same behavior in the higher part of the spectrum. This is a limitation caused by the assumption of isotropic turbulence that follows the use of the von Karman turbulence spectrum. Different results would be obtained by adopting other models of turbulence [39].

Finally, Fig. 5 reports the fast Fourier transform and the pressure time history obtained from the BEM + FW-H code described in Sect. 3, for the case of a wind speed of 11 m/s. Noise analysis is performed on a one-minute simulation time window sampled at a frequency of 50 Hz. Plots clearly show a main peak corresponding to the 3P frequency ($\sim$ 0.6 Hz). This peak is mainly caused by the influence of the tower on the loading noise, while thickness noise acts as a minor contributor to the overall sound. This is expected to be due to the low rotational speed. It can be also noted that loading noise has not a null mean, but it presents a constant offset. This term, which is called DC shift in [34], is negative on the suction side of the rotor and

Table 2: IEA Wind Task 37 characteristics

Data	**Value**
Wind class	IEC 3A
Control	Collect. Pitch
Rated electrical power	3.35 MW
Hub height H	110.0 m
Rotor radius R	65.0 m
Rotor cone angle Ξ	3.0 deg
Nacelle uptilt angle Φ	5.0 deg
Max blade tip speed $v_{\mathrm{tip}_{\mathrm{max}}}$	80.0 m/s
Blade mass	17,404 kg
Nominal AEP	13.95 GWh
CoE	46.87 $/MWh

Table 3: Test cases

Data @ 7 m/s	**Value**
Rotor speed Ω	8.67 rpm
Pitch β	0.97 deg
Power coefficient C_P	0.481
Computed OASPL	53.17 dB(A)

Data @ 11 m/s	**Value**
Rotor speed Ω	11.75 rpm
Pitch β	6.98 deg
Power coefficient C_P	0.333
Computed OASPL	56.36 dB(A)

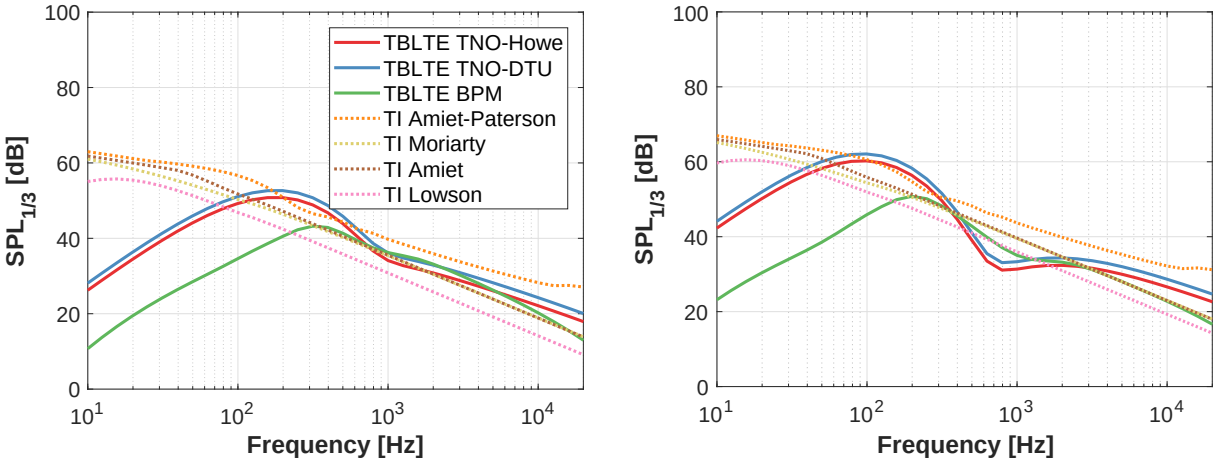

Figure 4: SPL spectra for the IEA Wind Task 37 computed at 7 m/s (left) and 11 m/s (right)

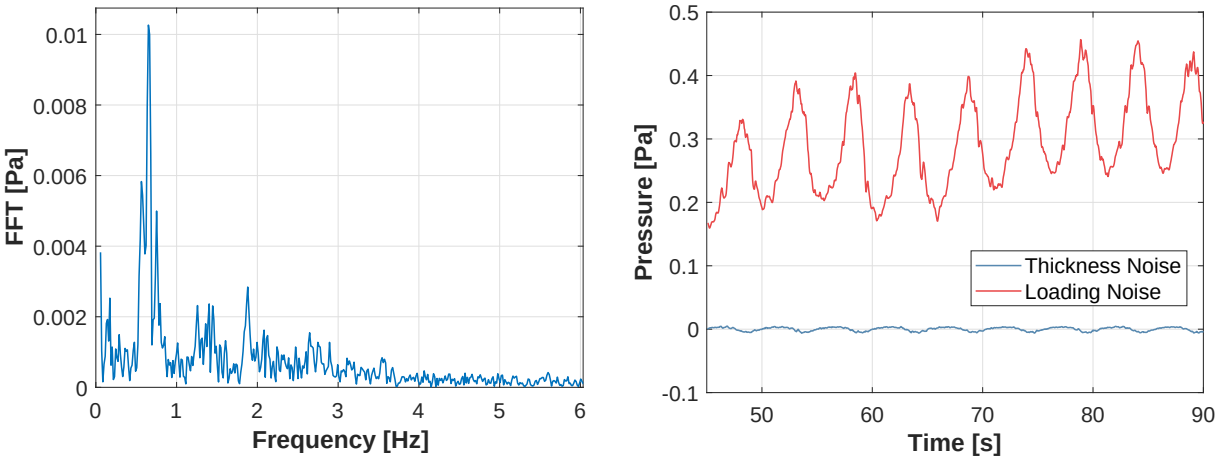

Figure 5: FFT of the acoustic pressure (left) and thickness and loading noise for one blade (right)

positive on the pressure side. Effects of turbulence are evident in the spectra and are caused by the changes in loading noise on the rotor. These effects disappear when a steady wind grid is employed.

5. Conclusions

In the present work, models for noise emission of wind turbines are compared, highlighting some major differences that exist among the various formulations presented in the literature. Several models for turbulent boundary layer – trailing edge and turbulent inflow noise are implemented within the same wind turbine design framework `Cp-Max`, which is based on a BEM aeroelastic solver. Noise spectra for different wind speeds are computed for the reference onshore wind turbine developed within IEA Wind Task 37. Discrepancies between the TNO and BPM models for the trailing edge noise are highlighted. These are attributed to the empirical nature of the BPM model, where typical wind turbine applications exceed the boundaries of applicability of the model.

In addition, a time-domain Ffowcs Williams-Hawkings is coupled to the same BEM based aeroelastic solver. The FW-H approach is well suited for the prediction of noise emissions in the low frequency regime. Indeed, results for the infrasound spectrum appear to be promising, correctly capturing the 3P harmonic.

The present work is so far only limited to the reporting and documenting of differences existing among models and formulations. Within the German national project TremAc [40], an experimental campaign is currently ongoing with the goal of assessing the emissions of an E82 ENERCON wind turbine in the range 0.1–20 kHz. As soon as experimental data becomes available, a validation of the models will be conducted. In addition, several limitations of the models should be addressed. First, the effects of the boundary layer transition position has not yet been investigated, while the free transition has so far only been set with the `XFOIL` internal e^N algorithm. Secondly, both frequency and time-domain methods make use of `XFOIL` to reconstruct loading or boundary layer characteristics of 2d sections, neglecting three-dimensional and unsteady effects. In addition, in the development of the FW-H model coupled to BEM aerodynamics, important phenomena for low-frequency noise have so far been neglected, such as sound absorption, ground reflection and wake flow field. All the above limitations should be carefully studied and addressed by the development of suitable models.

Acknowledgements

This research was supported by the German Federal Ministry for Economic Affairs and Energy (BMWi) within the TremAc (FKZ: 0325839D) project.

References

[1] Bortolotti P, et al. *The Science of Making Torque from Wind 2018*, Milano, Italy, 2018.
[2] Bottasso CL, et al. *Multib. Syst. Dyn.*, 2006;16(3):291-308. doi: 10.1007/s11044-006-9027-1
[3] Bortolotti P, Bottasso CL, Croce A. *Wind Energ. Sci.*, 2016;1(1):71-88. doi: 10.5194/wes-1-71-2016
[4] Ffowcs Williams JE, Hawkings DL. *Royal Society London*, 1968;264(1151). doi: 10.1098/rsta.1969.0031
[5] Brooks TF, Pope DS, Marcolini MA. Airfoil self-noise and prediction. *NASA Reference Publication 1218*, 1989.
[6] Oerlemans S, Sijtsma P, Méndez López B. *Journal of Sound and Vibration*, 2007. doi: 10.1016/j.jsv.2006.07.032
[7] Doolan CJ, Moreau DJ. *Int. J. of Aeroacoustics*, 2015;14(5-6):811-832. doi: 10.1260/1475-472X.14.5-6.811
[8] Herr M, et al. *Proc. 21st AIAA/CEAS Aeroacoustics Conference*, 2015. doi: 10.2514/6.2015-2847
[9] Lau ASH, et al. *Wind Energy*, 2017;20(10):1727-1752. doi: 10.1002/we.2119
[10] Parchen RR. Progress report draw : a prediction scheme for trailing edge noise based on detailed boundary layer characteristics. *Report TNO Institute of Applied Physics*, Delft, The Netherlands, 1998.
[11] Chandiramani KL. *The J. of the Acoustical Society of America*, 1974;55(1):19-29. doi: 10.1121/1.1919471
[12] Chase D. *AIAA Journal*, 1975;13(8):1041-1047. doi: 10.2514/3.60502
[13] Blake W. Mechanics of Flow-Induced Sound and Vibration, Vol.1. *Acad. Press*, 1986. ISBN: 9780128122891
[14] Lutz T, et al. *AIAA Journal*, 2007;45(4):779-785. doi: 10.2514/1.27658

[15] Bertagnolio F. Trailing edge noise model applied to wind turbine airfoils. *Tech. Rep. Risø-R-1633(EN)*, 2008.
[16] Moriarty P, et al. *11th AIAA/CEAS Aeroacoustics Conference*, 2005. doi: 10.2514/6.2005-2881
[17] Bertagnolio F, et al. *J. of Sound and Vibration*, 2014;333(3):991-1010. doi: 10.1016/j.jsv.2013.10.008
[18] Kamruzzaman M, et al. *AIAA Journal*, 2012;50(1):46-60. doi: 10.2514/1.J050805
[19] XFOIL Documentation, 2017 http://web.mit.edu/drela/Public/web/xfoil/
[20] Zhu WJ, et al. *J. of Solar Energy Engineering*, 2005;127(4):517-528. doi: 10.1115/1.2035700
[21] Moriarty P. NAFNoise User's Guide. 2005. `https://nwtc.nrel.gov/NAFNoise`.
[22] Bertagnolio F, et al. *Wind Energy*, 2017;20(8):13311348. doi: 10.1002/we.2096
[23] Howe MS. *J. of Sound and Vibration*, 1978;61(3):437-465. doi: 10.1016/0022-460X(78)90391-7
[24] Brooks TF, Hodgson TH. *J. of Sound and Vibration*, 1981;78(1):69-117. doi: 10.1016/S0022-460X(81)80158-7
[25] Amiet RK. *Journal of Sound and Vibration*, 1975;41(4):407-420. doi: 10.1016/S0022-460X(75)80105-2
[26] Paterson RW, Amiet RK. *3rd AIAA Aero-Acoustics Conference*, Palo Alto, CA, 1976. doi: 10.2514/6.1976-571
[27] Lowson MV. Assessment and prediction of wind turbine noise. *Flow Solutions Report 92/19*, 1993.
[28] Guidati G, et al. *3rd AIAA/CEAS Aeroacoustics Conference*, Atlanta,GA, 1997. doi: 10.2514/6.1997-1698
[29] Roger M, Moreau S. *Int. J. of Aeroacoustics*, 2010;9(3):273-305. doi: 10.1260/1475-472X.9.3.273
[30] Kim H, et al. *Renewable Energy*, 2012;42:46-53. doi: 10.1016/j.renene.2011.09.019
[31] Botha JDM, et al. Some noise predictions for small wind turbines. *Proc. ISMA 2016 - USD 2016*, 2016.
[32] IEC-61400-1 - Wind turbines - Part 1: Design requirements, Ed.3. 2005-08.
[33] Jonkman BJ. TurbSim User's Guide: V. 1.50. *NREL/TP-500-46198*, 2009. `https://nwtc.nrel.gov/TurbSim`
[34] Farassat F. Derivation of Formulations 1 and 1A of Farassat. *NASA/TM-2007-214853, L-19318*, 2007.
[35] Pitt DM, Peters DA. Theoretical prediction of dynamic-inflow derivatives. 1980.
[36] Amiet RK, Schlinker RH. *AIAA, Astrodynamics Specialist Conference*, 1981. doi: 10.2514/6.1981-2001
[37] Dykes K, et al. *IEA Task 37 Final Proposal*, 2015. `https://sites.google.com/site/ieawindtask37`
[38] IEC-61400-11 - Wind turbines - Part 11: Acoustic noise measurement techniques. 2006.
[39] Buck S, Oerlemans S, Palo S. *J. of Sound and Vibration*, 2016;385:219-238. doi: 10.1016/j.jsv.2016.09.010
[40] TremAc Consortium website: `http://www.windfors.de/english/tremac.html`